Toxicokinetic interaction between hepatic disposition and pulmonary bioactivation of inhaled naphthalene studied using *Cyp2abfgs*-null and CYP2A13/2F1-humanized mice with deficient hepatic cytochrome P450 activity

Nataliia Kovalchuk, Qing-Yu Zhang, Jacklyn Kelty, Laura Van Winkle, and Xinxin Ding

Department of Pharmacology and Toxicology, College of Pharmacy, University of Arizona, Tucson, AZ 85721 (N.K., Q.-Y.Z., X.D.); Wadsworth Center, New York State Department of Health, and School of Public Health, State University of New York at Albany, NY 12201 (N.K., Q.-Y.Z.); Center for Health and the Environment and Department of Anatomy Physiology and Cell Biology, School of Veterinary Medicine UC Davis, Davis, CA 95616 (J.K., L.V.); College of Nanoscale Science, SUNY Polytechnic Institute, Albany, NY 12203 (X.D.)

RUNNING TITLE: Disposition and bioactivation of inhaled naphthalene

ADDRESS MANUSCRIPT CORRESPONDENCE TO:

Dr. Xinxin Ding, Department of Pharmacology and Toxicology, College of Pharmacy, University of Arizona, Tucson, AZ 85721.

Tel. (520) 626-9906; E-mail: xding@pharmacy.arizona.edu

Number of Text Pages:	24
Number of Tables:	2
Number of Figures:	6
Number of References:	33
Number of words	
Abstract:	250
Significance:	102
Introduction:	747
Discussion:	1472

ABBREVIATIONS: NA, naphthalene; Cpr, cytochrome P450 reductase; LCN, liver-Cpr-null; WT, wild-type; GSH, glutathione; NADPH, β-nicotinamide adenine dinucleotide phosphate; AP-GSH, acetaminophen-glutathione conjugate; NA-GSH, naphthalene-glutathione conjugate; CL, clearance; $t_{1/2}$, elimination half-life; and FA, filtered air.

*Corresponding authors: X. Ding (xding@pharmacy.arizona.edu) and L. Van Winkle (lsvanwinkle@ucdavis.edu)

ABSTRACT

Previous studies using *Cyp2abfgs*-null (lacking all genes of the *Cyp2a*, *2b*, *2f*, *2g*, and *2s* subfamilies), CYP2A13/2F1-humanized, and liver-*Cpr*-null (LCN) mice showed that, whereas hepatic P450-enzymes are essential for systemic clearance of inhaled naphthalene, a possible human carcinogen, both hepatic and extrahepatic P450s may contribute to naphthalene-induced lung toxicity via bioactivation. Herein, we aimed to further understand the toxicokinetics of inhaled naphthalene, to provide a basis for predicting the effects of variations in rates of xenobiotic disposition on extent of target tissue bioactivation. We assessed the impact of a hepatic deficit in naphthalene metabolism on the toxicokinetics of inhaled naphthalene using newly generated "*Cyp2abfgs*-null-and-LCN" and "CYP2A13/2F1-humanized-and-LCN" mice. We determined plasma, lung and liver levels of naphthalene and naphthalene-glutathione conjugate, a biomarker of naphthalene bioactivation, over time following naphthalene inhalation. We found that the loss of hepatic naphthalene metabolism severely decreased naphthalene systemic clearance and caused naphthalene to accumulate in the liver and other tissues. Naphthalene release from tissue, as evidenced by continued increase in plasma naphthalene levels after termination of active inhalation exposure, was accompanied by prolonged bioactivation of naphthalene in the lung. Additionally, transgenic expression of human CYP2A13/2F1 in the respiratory tract caused a reduction in plasma naphthalene levels (by 40%, relative to "*Cyp2abfgs*-null-and-LCN") and corresponding decreases in naphthalene-glutathione levels in the lung in mice with hepatic P450 deficiency, despite the increase in local naphthalene-bioactivating P450 activity. Thus, the bioavailability of naphthalene in the target tissue has a significant effect on the extent of naphthalene bioactivation in the lung.

SIGNIFICANCE STATEMENT

In this study, we report several novel findings related to the toxicokinetics of inhaled naphthalene, the ability of which to cause lung carcinogenesis in humans is a current topic for risk assessment. We show accumulation of naphthalene in liver and lung in mice with compromised hepatic P450 activity; ability of tissue-stored naphthalene to redistribute to the circulation after termination of active inhalation exposure, prolonging exposure of target tissues to naphthalene; and ability of non-CYP2ABFGS enzymes of the lung to bioactivate naphthalene. These results suggest potentially large effects of deficiencies in hepatic P450 activity on naphthalene tissue burden and bioactivation in human lungs.

Introduction

Naphthalene (NA) is present ubiquitously in the environment (Witschi et al., 1997; Kakareka and Kukharchyk, 2003). High exposure to NA occurs in occupational settings (Preuss et al., 2003; Chao et al., 2006). Urinary naphthol levels were elevated in the post-shift, compared to pre-shift, period among exposed workers (Serdar et al., 2004; McClean et al., 2012; Merchant-Borna et al., 2012), providing evidence for NA metabolism in humans. NA metabolism by human liver microsomes has also been documented (Tingle et al., 1993; Wilson et al., 1996). However, the question remains whether NA-induced respiratory tract toxicity, as has been found in animal models (Warren et al., 1982; Abdo et al., 1992; Abdo et al., 2001), occurs in the human respiratory tract. There are no clear-cut human epidemiological data on the long-term effects of NA exposure because human NA exposures are often as a part of mixtures (Griego et al., 2008).

The toxic effects of NA are dependent on CYP-mediated bioactivation via NA-oxide formation (Buckpitt et al., 2002). CYP2F2, expressed predominantly in mouse airways and in liver, has the lowest K_m among CYPs studied for NA bioactivation (Shultz et al., 1999), and plays a dominant role in NA-induced pulmonary damage (Verschoyle et al., 1997; Genter et al., 2006; Li et al., 2011). In contrast, CYP2A5, abundantly expressed in the mouse nasal olfactory mucosa, lung, and liver, is the main contributor to NA-induced nasal toxicity (Hu et al., 2014). Human CYP2F1 and CYP2A13 are mainly expressed in the respiratory tract in humans, with negligible expression in other tissues (Su et al., 2000; Carr et al., 2003; Weems and Yost, 2010). Metabolism of inhaled NA by respiratory-tract expressed transgenic CYP2F1 and CYP2A13 resulted in cytotoxicity in lung airway epithelia and nasal olfactory mucosa in CYP2A13/2F1-humanized mice, highlighting potential impact of the human enzymes on NA metabolism and respiratory-tract toxicity (Li et al., 2017).

Several P450 isoforms with ability to metabolize NA are also identified in human liver, including CYP1A2, CYP2A6, CYP3A4, and CYP2D6 (Cho et al., 2006; Shimada et al., 2016). Hepatic P450-mediated NA metabolism has a major impact on the in vivo disposition of inhaled or intraperitoneally administered NA, as indicated by studies comparing wild type (WT) and liver-*Cpr*-null (LCN) mice (Li et al., 2011; Kovalchuk et al., 2017). However, both hepatic and extrahepatic P450-mediated NA metabolism also contributed to toxicity in lung airways following inhalation exposure to NA at occupationally relevant concentrations (Kovalchuk et al., 2017). These seemingly opposing actions of hepatic P450-mediated NA metabolism make it complicated to predict consequences of alterations in hepatic NA metabolism on risks of lung toxicity. It is also unclear to what degree circulating NA can influence the extent of target tissue NA bioactivation in an inhalation exposure model, where the lung is directly exposed to NA in the inhaled air, or whether extrahepatic organ NA metabolism contributes significantly to systemic disposition of NA when hepatic P450 activity toward NA is deficient. Thus, a better understanding of the relationships between hepatic P450 activity, which may vary due to induction, inhibition, disease conditions, or genetic polymorphism, and the toxicokinetics of NA following inhalation exposure might help with prediction of the risks of NA toxicity in individuals with compromised hepatic P450 activity.

In the current study, we aimed to study the impact of a hepatic deficit in NA metabolism on the toxicokinetics of inhaled NA. The hepatic deficit was modeled using LCN mice, which undergo tissue-specific deletion of the *Cpr* gene in hepatocytes, resulting in tissue-specific ablation of nearly all microsomal P450 activities in the liver (Gu et al., 2003). We crossbred the LCN mice with mice that are "humanized" by having a much lower overall rate of NA metabolism in the lung (relative to WT mice), because of germline (whole body) deletion of the *Cyp2abfgs* gene cluster

(including all genes in the *Cyp2a*, *Cyp2b*, *Cyp2f*, *Cyp2g* and *Cyp2s* subfamilies) (Li et al., 2014), and by expressing human CYP2A13 and CYP2F1 (Wei et al., 2012). We exposed CYP2A13/2F1-humanized and *Cyp2abfgs*-null mice with either normal or compromised hepatic P450s activity ("*Cyp2abfgs*-null and LCN" and "CYP2A13/2F1-humanized and LCN") to inhaled NA at an occupationally relevant concentration (10 ppm). We then determined the levels of NA and NA-glutathione (GSH) conjugate, a biomarker of P450-catalyzed NA bioactivation via NA oxide formation, in plasma, liver and lung at various times following termination of inhalation exposure. The toxicokinetic data from these various mouse strains were compared, to identify the roles of hepatic and respiratory tract P450 enzymes in NA distribution, bioactivation, and disposition.

Material and Methods

Chemicals and reagents

NA (CAS# 91-20-3, purity 99%), NA-d_8 (CAS# 1146-65-2, purity 99%), GSH (CAS# 70-18-8, purity ≥ 98.0%), and β-nicotinamide adenine dinucleotide phosphate, reduced tetra(cyclohexyl ammonium) salt (NADPH) (CAS#, 100929-71-3, purity ≥ 95.0%), were purchased from Sigma Aldrich (St. Louis, MO). Acetaminophen-glutathione (AP-GSH) was purchased from Toronto Research Chemicals (Toronto, ON, Canada). NA-GSH standard as a mixture of all four stereoisomers was a generous gift from Drs. Alan R. Buckpitt and Dexter Morin (University of California at Davis, Davis, CA) and was prepared as previously described (Richieri and Buckpitt, 1987). All solvents (dichloromethane, formic acid, methanol and water) were of analytical grade (Fisher Scientific, Houston, TX).

Mouse breeding and characterization

Cyp2abfgs$^{-/-}$ (*Cyp2abfgs*-null), CYP2A13/2F1-TG$^{+/-}$/*Cyp2abfgs*$^{-/-}$ (CYP2A13/2F1-humanized), and LCN (albumin-Cre/*Cpr*$^{lox/lox}$) mice, male and female, all on C57BL/6 background, were obtained from breeding stocks maintained at the Wadsworth Center. Progeny of *Cyp2abfgs*-null and LCN intercrosses were further intercrossed with CYP2A13/2F1-humanized mice to generate "CYP2A13/2F1-humanized and LCN" and "*Cyp2abfgs*-null and LCN" mice. A detailed breeding scheme is presented in Figure 1A. All pups were genotyped using tail DNA for the presence of the Cre transgene, the loxP sites, and the *Cyp2f2*$^{+}$, *Cyp2abfgs*$^{-}$, and the CYP2F1^{+} alleles. For genotype analysis, PCR was carried out for 35 cycles with annealing temperature at 60ºC for 30 seconds and extension at 72ºC for 1 minute for each cycle. The list of PCR primers for, and representative results of, the genotyped alleles are presented in Supplementary Table 1

and Figure 1B, respectively. PCR products were separated by electrophoresis in agarose gels and visualized after staining with ethidium bromide.

Serum levels of albumin, blood urea nitrogen, total bilirubin, alkaline phosphatase, alanine aminotransferase, and cholesterol were estimated for naïve *Cyp2abfgs*-null, CYP2A13/2F1-humanized, "*Cyp2abfgs*-null and LCN" and "CYP2A13/2F1-humanized and LCN" male mice, with a VETSCAN VS2 Chemistry Analyzer, using the Mammalian Liver Profile rotors (Abaxis, Union City, CA). A 100-µL aliquot of serum from each mouse was analyzed.

Assay for NA bioactivation in vitro

The rate of NA-GSH formation was measured according to a previously described protocol (Shultz et al., 1999). Microsomes were prepared from individual livers, pooled lungs, or pooled olfactory mucosa of male, 2-3-month old mice. Reaction mixtures contained 50 mM phosphate buffer (pH 7.4), NA (100 µM, added in 1 µL methanol), 10 mM GSH, 1 mM NADPH, and different concentrations of microsomal proteins (0.2 mg/mL for liver, 0.25 mg/mL for olfactory mucosa and 1 mg/mL for lung), in a final volume of 0.1 mL. The reactions were carried out in tightly capped glass tubes (2-dram vials) at 37ºC for 10 min for liver, 30 min for olfactory mucosa, and 60 min for lung microsomal proteins. The reaction was quenched by transferring the incubation tubes to an ice bath and adding to the uncapped tubes 0.2 mL of ice-cold methanol containing the internal standard AP-GSH. The resultant mixtures were centrifuged twice to remove precipitated proteins and aliquots of supernatants were injected into UPLC-MS/MS for analysis, as previously described (Kovalchuk et al., 2017). NADPH, GSH, or NA were omitted, or boiled microsomes were used, in negative control incubations.

Animal exposure

All animal studies were approved by the Institutional Animal Care and Use Committee of the Wadsworth Center. Two- to three-month old male mice were used for the study. NA inhalation exposure settings were the same as described in details elsewhere (Kovalchuk et al., 2017). Mice were nose-only exposed to a single 4-hour session of 10 ppm NA (OSHA-established exposure limit for occupational settings) or HEPA-filtered air (sham-exposure control) in an Oral Nasal Aerosol Respiratory Exposure System (CH Technologies, Westwood, NJ). Male mice were chosen for the study, to be consistent with previous studies on NA lung toxicity (Kovalchuk et al., 2017; Li et al., 2017).

For plasma toxicokinetics studies, blood samples (20-25 µl) were collected via tail vein from each mouse (n=3-4 per each genotype) at multiple time points (0, 1, 4, 8 and 20 hours) after termination of NA exposure. For tissue toxicokinetics studies, mice of all four genotypes were exposed simultaneously for each time point (n=3-5 per each genotype for each time point), and different mice are used for different time points. Tissues (lung and liver) were collected at 0, 2, 6, or 20 h postexposure, quick-frozen on dry ice, and stored in sealed tubes at -80^{o}C until analysis.

Detection of NA and NA-GSH

For NA detection, plasma (10 µL) or lung homogenates (50 µL) were spiked with NA-d_8 and extracted with dichloromethane (100 µL for plasma and 110 µL for tissue) as previously described (Kovalchuk et al., 2017). GC-MS detection of NA (m/z 128) and NA-d_8 (m/z 136) was carried out using Agilent Technologies model 5975 C inert XL EI/CI mass spectrometer (Agilent, Santa Clara, CA), which was interfaced with an Agilent model 7890 A gas chromatography system and operated in the selected ion monitoring mode (SIM) using electron impact ionization. The

extract (1 µl) was injected in splitless mode, with the inlet at 260ºC. Analytes were separated on a Restek Rxi-5ms (30 m x 0.25 mm; 0.25 µm) column (Restek, Bellefonte, PA) under a constant flow (1 mL/min) of helium (Li et al., 2011). Blank plasma and blank tissue homogenate from naïve mice were spiked with freshly prepared NA standards (5-500 ng/mL) and NA-d_8 (5 ng in 10 µL of methanol). Ratios of detected NA and NA-d_8 were used to plot matrix-specific calibration curves and quantify NA in samples. The assay variability (relative SD) did not exceed 15%; the limit for NA quantification (signal to noise ratio > 10) was 5 pg on column.

For NA-GSH detection, reaction mixtures (100 µL), plasma (10 µL), or tissue homogenates (50 µL) were spiked with an internal standard AP-GSH, and mixed with methanol (200, 80 and 90 µL, respectively) for protein precipitation, as described previously (Kovalchuk et al., 2017). NA-GSH and AP-GSH were separated at room temperature on an Agilent Elipse Plus C18 (2.1 x 50 mm; 1.8 µm) column at a flow rate of 0.2 mL/min with a mobile phase as previously described (Li et al., 2011), using an Agilent model 1290 Infinity Series ultra-performance liquid chromatography system. Analyte ions were detected using an AB-SCIEX model 6500 Q-Trap mass spectrometer (AB-SCIEX, Framingham, MA) in the positive ion mode using multiple reaction monitoring (MRM) scanning. The transitions for NA-GSH quantification were M/Z 452/306 and M/Z 452/288 (confirmatory), and, for AP-GSH quantification, it was M/Z 457/328.

Matrix-matched calibration curves were prepared over the range of 5-227 ng/mL NA-GSH. AP-GSH (0.55 ng in 10 µL of methanol) was added to each sample. The assay variability (relative SD) did not exceed 15%. The limit for NA-GSH quantification (signal-to-noise ratio >10) was 10 pg on column.

Calculations and Statistics

DMD Fast Forward. Published on October 8, 2019 as DOI: 10.1124/dmd.119.088930
This article has not been copyedited and formatted. The final version may differ from this version.

The bicinchoninic acid assay was used to quantify total protein concentration (Pierce Chemical, Rockford, IL) using bovine serum albumin as a standard. Pharmacokinetic parameters (area under the curve (AUC), elimination half-live ($t_{1/2}$), and clearance) were calculated using the WinNonlin software (Pharsight, Mountain View, CA), with use of a non-compartmental model. Statistical significance of differences among study groups in various parameters was analyzed by one-way or two-way ANOVA, followed by Bonferroni's test for multiple comparisons, using GraphPad Prizm software (GraphPad, San Diego, CA).

Results

Generation and characterization of "CYP2A13/2F1-humanized and LCN" and "*Cyp2abfgs*-null and LCN" mice

"*Cyp2abfgs*-null and LCN" and "CYP2A13/2F1-humanized and LCN" mice were progeny of intercrosses between *Cyp2abfgs*$^{-/-}$ (*Cyp2abfgs*-null), liver-*Cpr*-null (LCN), and CYP2A13/2F1-TG$^{+/-}$/*Cyp2abfgs*$^{-/-}$ (CYP2A13/2F1-humanized) mice (Fig. 1A). In "*Cyp2abfgs*-null and LCN" and "CYP2A13/2F1-humanized and LCN" mice, the expression of Cre recombinase, driven by the rat albumin promoter, results in hepatocyte-specific deletion of the *Cpr* gene sequence between exons 3 and 15 (Wu et al., 2003) and, as has been shown previously (Gu et al., 2003), significantly lowered levels of CPR protein expression in the whole liver (Supplementary Fig. 1).

"*Cyp2abfgs*-null and LCN" and "CYP2A13/2F1-humanized and LCN" mice are normal in growth, development, general appearance, daily activity and reproduction. Body weights and weights of lung, kidney, brain, and heart of 2-month-old "*Cyp2abfgs*-null and LCN" and "CYP2A13/2F1-humanized and LCN" mice were unchanged, compared to those of *Cyp2abfgs*-null and CYP2A13/2F1-humanized mice (Supplementary Table 2). However, enlargement of the liver was observed in the "*Cyp2abfgs*-null and LCN" and "CYP2A13/2F1-humanized and LCN" male mice (1.98±0.33 g and 2.12±0.18 g, respectively). These values are comparable to the values previously reported for 2-month-old, male LCN mice (2.04±0.49 g) (Gu et al., 2003), but significantly greater than the liver weights in *Cyp2abfgs*-null and CYP2A13/2F1-humanized mice (1.25±0.12 g and 1.21±0.11 g, respectively). Similar to what was reported previously for the LCN mice, there was a significant increase in serum alanine aminotransferase (~2-fold) and a decrease in serum cholesterol (~2-fold) in "*Cyp2abfgs*-null and LCN" and "CYP2A13/2F1-humanized and LCN" mice compared to *Cyp2abfgs*-null and CYP2A13/2F1-humanized mice, respectively (Supplementary Figure 2, panels A, B). Serum alkaline phosphatase level was also increased (by

~2-fold), but there was no change in serum levels of albumin, blood urea nitrogen, or total bilirubin (Supplementary Figure 2, panels C-F).

Liver, lung, and nasal microsomal CYP-mediated NA bioactivation in vitro

To assess the relative activities of different organs to metabolize NA in the various mouse strains, we compared the rates of microsomal NA-GSH formation in livers, lung (whole lung), and olfactory mucosa of "CYP2A13/2F1-humanized and LCN" and "*Cyp2abfgs*-null and LCN" mice, with NA at a saturating concentration (100 μM). As shown in Table 1, lung and liver microsomal activities were significantly lower than in olfactory mucosa ($p<0.0001$), in both mouse strains, but the difference was much greater in the "CYP2A13/2F1-humanized and LCN" than in "*Cyp2abfgs*-null and LCN" mice.

Genotype-dependent difference in ability to bioactivate NA *in vitro* was observed in microsomes from olfactory mucosa and lungs (where the human CYP2A13 and CYP2F1 transgenes were expressed in the "CYP2A13/2F1-humanized and LCN" mice, but not in the "*Cyp2abfgs*-null and LCN" mice), but not in liver (where the human transgenes were not expressed and Cpr expression was abolished). Lung microsomes from "CYP2A13/2F1-humanized and LCN" mice had greater ability to bioactivate NA than "*Cyp2abfgs*-null and LCN" mice, by 67%. This genotype-dependent difference was more prominent for microsomal activities of the nasal olfactory mucosa (3.9-fold higher in "CYP2A13/2F1-humanized and LCN" than in "*Cyp2abfgs*-null and LCN"). Overall, these data confirm that the activities of the nasal and lung microsomes in the "CYP2A13/2F1-humanized and LCN" and "*Cyp2abfgs*-null and LCN" mice were like what was previously found in the CYP2A13/2F1-humanized and *Cyp2abfgs*-null mice, respectively (Li et al., 2017); whereas the activities of the liver microsomes of the two new strains were similar to what was found in the original LCN mice (Kovalchuk et al., 2017) (Table 1). Thus, the nasal and

DMD Fast Forward. Published on October 8, 2019 as DOI: 10.1124/dmd.119.088930
This article has not been copyedited and formatted. The final version may differ from this version.

lung microsomal NA oxidation activities (and by inference the transgenic CYP2A13/2F1 expression) were not altered by hepatic CPR status.

NA and NA-GSH levels in the plasma of "CYP2A13/2F1-humanized and LCN" and "*Cyp2abfgs*-null and LCN" mice

Levels of NA and NA-GSH were measured in the plasma of CYP2A13/2F1-humanized, *Cyp2abfgs*-null, "CYP2A13/2F1-humanized and LCN" and "*Cyp2abfgs*-null and LCN" mice, at multiple time points, starting immediately after termination of a single 4-hour inhalation exposure to 10-ppm NA. Levels of NA in the plasma of mice with abolished hepatic CPR expression ("CYP2A13/2F1-humanized and LCN" and "*Cyp2abfgs*-null and LCN") were significantly higher ($p<0.001$) compared to corresponding controls with normal hepatic CPR expression (CYP2A13/2F1-humanized and *Cyp2abfgs*-null) during the first eight hours after termination of NA exposure (Fig. 2A, 2C). Notably, NA levels in plasma continued to increase in "CYP2A13/2F1-humanized and LCN" and "*Cyp2abfgs*-null and LCN" mice after termination of active NA inhalation exposure. The trend of NA elevation was similar between the two mouse strains on LCN background, although the observed NA elevation during the first four hours after NA exposure termination, compared to the 0-hour time point, was statistically significant only for "*Cyp2abfgs*-null and LCN" mice ($p<0.05$). There was also a small, but statistically significant, difference ($p<0.05$) in NA plasma level between "CYP2A13/2F1-humanized and LCN" and "*Cyp2abfgs*-null and LCN" mice at 4 and 8 hours after termination of NA exposure (Fig. 2E). Unlike the relatively steady plasma NA levels during first eight hours after NA exposure termination in mice on LCN background, NA levels in the plasma of mice with normal hepatic CPR expression (CYP2A13/2F1-humanized and *Cyp2abfgs*-null) declined rapidly during the first

DMD Fast Forward. Published on October 8, 2019 as DOI: 10.1124/dmd.119.088930
This article has not been copyedited and formatted. The final version may differ from this version.

four hours after termination of NA exposure (Fig. 2A, 2C), and there was no difference between CYP2A13/2F1-humanized and *Cyp2abfgs*-null (Fig. 2G).

The levels of NA-GSH in the plasma immediately after termination of NA inhalation exposure were similar among the four different genotype groups, which had either normal or compromised hepatic CPR expression (Fig. 2B, 2D). Levels of NA-GSH declined rapidly in the plasma of CYP2A13/2F1-humanized mice and *Cyp2abfgs*-null mice, approaching detection limit (0.6 pmol on column) by 8 hours after termination of NA exposure; there was no difference between the two strains (Fig. 2H). In contrast, relatively high and constant levels of NA-GSH were maintained in the plasma of "CYP2A13/2F1-humanized and LCN" mice and "*Cyp2abfgs*-null and LCN" mice during the first 8 hours after termination of NA exposure (Fig. 2F), which coincided with elevated and steady plasma NA levels during the same post-exposure time period (Fig. 2E). Additionally, "CYP2A13/2F1-humanized and LCN" mice showed a trend of lower plasma NA-GSH levels, compared to "*Cyp2abfgs*-null and LCN" mice (Fig. 2F).

Toxicokinetic analysis of the data from Figure 2 (Table 2) revealed ~2.8-fold higher Cmax values for NA in mice with compromised hepatic CPR expression than in mice with normal hepatic CPR expression. The AUC values for NA were ~36-fold higher in "CYP2A13/2F1-humanized and LCN" than in CYP2A13/2F1-humanized mice and ~66-fold higher in "*Cyp2abfgs*-null and LCN" than in *Cyp2abfgs*-null mice. There was a ~1.7-fold increase ($p<0.05$) in AUC for NA levels in "*Cyp2abfgs*-null and LCN" mice, compared to "CYP2A13/2F1-humanized and LCN" mice. The rate of NA clearance (Cl/F) was significantly decreased in "CYP2A13/2F1-humanized and LCN" and "*Cyp2abfgs*-null and LCN" (~ 64-fold and ~66-fold, respectively), compared respectively to CYP2A13/2F1-humanized and *Cyp2abfgs*-null mice. In addition, plasma elimination half-life ($t_{1/2}$) of NA was substantially increased in "CYP2A13/2F1-humanized and

LCN" (by ~18-fold) and "*Cyp2abfgs*-null and LCN" (by ~12-fold) over CYP2A13/2F1-humanized and *Cyp2abfgs*-null mice, respectively. The AUC values for NA-GSH were also increased (by ~7.8-fold) in "CYP2A13/2F1-humanized and LCN" compared to CYP2A13/2F1-humanized, and (by ~5.7-fold) in "*Cyp2abfgs*-null and LCN" compared to *Cyp2abfgs*-null mice.

NA and NA-GSH levels in the lung of "CYP2A13/2F1-humanized and LCN" and "*Cyp2abfgs*-null and LCN" mice

Levels of NA and NA-GSH were determined in lungs of mice with normal or compromised hepatic CPR expression at different time points after termination of inhalation exposure to 10 ppm NA. Level of NA immediately after termination of NA inhalation exposure was 3.9-fold higher in "CYP2A13/2F1-humanized and LCN" than in CYP2A13/2F1-humanized and 3.5-fold higher in "*Cyp2abfgs*-null and LCN" than in *Cyp2abfgs*-null mice (Fig. 3A, 3C). For mice of all four genotypes, NA levels in the lung (Fig. 3) were estimated (by assuming 1 ml plasma to be 1 g in weight) to be ~4-fold to 6-fold higher than in the plasma (Fig. 2) at 0-hour postexposure (see Fig. 4A for a direct comparison). In addition, there was a trend of higher NA level in lungs of *Cyp2abfgs*-null than in CYP2A13/2F1-humanized mice regardless of their hepatic CPR status (33% and 23% higher in mice with normal and compromised hepatic CPR expression, respectively) (Fig. 3E, 3G). Levels of NA in the lungs of CYP2A13/2F1-humanized and *Cyp2abfgs*-null mice decreased rapidly, being undetectable at 6 hours after termination of NA exposure (Fig. 3A, 3C). In contrast, NA levels in the lungs of mice with compromised hepatic CPR expression decreased slowly and remained relatively high at 6 hours after termination of active NA exposure (Fig. 3E).

NA-GSH levels in the lung were nearly identical in all groups of NA-exposed mice immediately after exposure termination despite significant difference in NA levels in plasma and tissues between mice with normal and compromised hepatic CPR expression. Levels of NA-GSH in lungs decreased significantly ($p<0.01$) at 2-hour postexposure in mice with normal hepatic CPR expression (Fig. 3H); but they were relatively steady in mice with compromised hepatic CPR expression (Fig. 3F). NA-GSH adducts were not detected at 6-hour postexposure in CYP2A13/2F1-humanized and *Cyp2abfgs*-null, in contrast to the "CYP2A13/2F1-humanized and LCN" and "*Cyp2abfgs*-null and LCN" mice, in which NA-GSH levels became non-detectable only at the 20-hour postexposure time point. For mice of all four genotypes, NA-GSH levels in the lung (Fig. 3) were estimated (by assuming 1 ml plasma to be 1 g in weight) to be higher than in the plasma (Fig. 2) at 0-hour postexposure (see Fig. 4B for a direct comparison).

NA and NA-GSH levels in the liver of "CYP2A13/2F1-humanized and LCN" and "*Cyp2abfgs*-null and LCN" mice

Hepatic NA levels were 20-fold higher in "CYP2A13/2F1-humanized and LCN" than in CYP2A13/2F1-humanized mice and 27-fold higher in "*Cyp2abfgs*-null and LCN" than in *Cyp2abfgs*-null mice immediately after termination of a 4-hour inhalation exposure (10 ppm) (Fig. 5A, 5C). Moreover, NA levels appeared to be higher (by 33%, $p=0.0632$) in the liver of "*Cyp2abfgs*-null and LCN" mice, compared to "CYP2A13/2F1-humanized and LCN" mice (Fig. 5E), at 0-h postexposure. NA levels were somewhat lower in livers (Fig. 5) than in lungs (Fig. 3) of mice with normal hepatic CPR expression, by 40% in *Cyp2abfgs*-null mice and 20% in CYP2A13/2F1-humanized mice, immediately after the inhalation exposure; but they were substantially higher in the liver than in the lung of "*Cyp2abfgs*-null and LCN" (by 4.5 fold) and

"CYP2A13/2F1-humanized and LCN" mice (by 3.4 fold) (see Fig. 6A for a direct comparison). NA levels in the liver of mice with normal hepatic CPR expression declined rapidly after termination of active NA exposure, being undetectable 6 hours after termination of NA exposure (Fig. 5G). In contrast, relatively steady NA levels were found in mice with compromised hepatic CPR expression during the first 6 hours of postexposure time, with a trend of higher NA levels in the "*Cyp2abfgs*-null and LCN" mice (Fig. 5E).

Levels of hepatic NA-GSH were ~2.5-fold higher in *Cyp2abfgs*-null than in "*Cyp2abfgs*-null and LCN" and ~2.6-fold higher in CYP2A13/2F1-humanized than in "CYP2A13/2F1-humanized and LCN" mice at 0-hour postexposure (Fig. 5B, 5D). The NA-GSH levels decreased more rapidly in mice with normal hepatic CPR expression (Fig. 5H) than in mice with abolished hepatic CPR expression (Fig. 5F), resulting in disappearance of CPR-genotype-related differences by the 2-hour time point and drastically lower NA-GSH levels in mice with normal hepatic CPR expression by the 6-hour time point. However, the adduct levels were not notably different between "CYP2A13/2F1-humanized and LCN" and "*Cyp2abfgs*-null and LCN" mice (Fig. 5F), or between CYP2A13/2F1-humanized and *Cyp2abfgs*-null mice (Fig. 5H). For mice of all four genotypes, NA-GSH levels in the liver (Fig. 5) were higher than in the lung (Fig. 3) at 0-hour postexposure (see Fig. 6B for a direct comparison).

DMD Fast Forward. Published on October 8, 2019 as DOI: 10.1124/dmd.119.088930
This article has not been copyedited and formatted. The final version may differ from this version.

Discussion

The extent of xenobiotic toxicity in a portal-of-entry, extra-hepatic organ is influenced by many factors, ranging from environmental exposure, absorption, and systemic exposure, to metabolic disposition via the target organ and the liver, and toxic metabolites generation either locally or systemically. In this study, we have examined NA disposition and bioactivation in mouse models undergoing genetic modulation of systemic metabolism of NA by the CYP2A, 2B, 2F, 2G, 2S enzymes, of hepatic metabolism by all microsomal P450 enzymes (LCN), and/or of expression of two human enzymes (CYP2A13 and 2F1) active toward NA metabolism in the respiratory tract.

The toxicokinetics of xenobiotics in an inhalation exposure model needs to be analyzed in two different time segments: during and after active inhalation exposure. During active inhalation exposure, absorption from the airways to the lung and blood is the dominant event but a steady-state plasma level is presumably established eventually, which reflects the sum of contributions by all absorption, distribution, metabolism, and excretion events occurring in the body. This level can be approximated by the level detected at the termination of active inhalation exposure (e.g., the 0-h data-point in Figure 2). Once inhalation exposure has been terminated, disposition via metabolism and excretion is the driving force that causes plasma and tissue levels to decrease, which includes evaporation from the airway surface for volatile compounds like NA as well as metabolism of circulating NA by P450 enzymes in the liver and extrahepatic organs,. This postexposure “decay” was rapid for NA in mice with normal hepatic P450 activities, as has been reported previously in other mouse models (Li et al., 2011; Kovalchuk et al., 2017), but much slower in mice with liver specific loss of CPR expression (Figures 2A, 2C). Furthermore, during active exposure, the steady-state NA levels in the liver, lung, and plasma were also much elevated

in mice with deficient liver P450 activity, presumably because of the decreased rate of metabolic disposition of circulating NA in the liver.

Interestingly, while NA levels in liver and lung decreased with postexposure time, plasma levels of NA continued to increase after the termination of inhalation exposure in mice with deficient hepatic P450 activities (Fig. 2A, 2C), a fact indicating redistribution of stored NA from other sites within the body to blood. Given that NA levels in the liver are so much higher than in the lung and plasma (Fig. 4, 6), and the ability of NA to diffuse through membranes, it can be deduced that the liver and possibly other extra pulmonary tissues not examined here, such as adipose tissue, are the major source of this postexposure increase in plasma NA levels and the main cause for the prolonged occurrence of NA exposure and bioactivation in the lung after (nose-only) inhalation exposures have ceased. This ability of inhaled NA to accumulate in the liver at high levels during active exposure and then be slowly released to the circulation and the target tissue for toxicity (lung) over many hours (Fig. 2, 5), in cases where hepatic P450 activity is suppressed, has important implications for predicting risks of lung toxicity from NA exposure in individuals with compromised hepatic P450 function. In that regard, hepatic P450 activities toward xenobiotic metabolism can be suppressed not only by CYP genetic polymorphism or drug-xenobiotic interactions, but also by various liver diseases (George et al., 1995; Frye et al., 2006).

Our data further suggested that increases in NA circulating or tissue levels during active inhalation exposure to NA did not have a significant impact on the extent of target tissue NA bioactivation in the lung. The levels of NA-GSH in the lungs of *Cyp2abfgs*-null or CYP2A13/2F1-humanized mice were the same regardless of whether liver P450 was functional (Fig. 3B, 3D) and despite significant differences in plasma (Fig. 2A, 2C) or lung NA levels (Fig. 3A, 3C) at the termination of active NA exposure. This intriguing observation may be explained by saturation of

the lung P450 enzymes by NA, which might be at very high levels in the airway and alveolar epithelial cells, during active exposure (10 ppm). However, the impact of circulating and tissue levels of NA on extent of NA bioactivation in the lung during postexposure period was obvious, given the LCN-genotype-related differences in tissue NA-GSH levels at 2 and 6 h following termination of NA exposure (Fig. 3B, 3D). It remains to be determined whether the same cells or lung regions are involved in NA metabolism during both active exposure and postexposure periods, as it is not clear whether circulating NA and airborne NA would be absorbed by lung tissue at differing sites.

It should also be noted that, in the LCN mice, with intact CYP2ABFGS enzymes in the lung, increases in circulating or tissue NA levels during active inhalation exposure to NA was accompanied by a significant increase in the extent of target tissue NA bioactivation in the lung (Kovalchuk et al., 2017). This earlier finding suggested that the lung P450 enzymes were not saturated by NA. The apparent discrepancy on effects of LCN status on WT (Kovalchuk et al., 2017) or *Cyp2abfgs*-null background (this study) is most likely because of a much lower lung tissue NA levels achieved in the LCN mice than in "*Cyp2abfgs*-null and LCN" mice, though differences in enzyme kinetic properties between CYP2ABFGS enzymes (more efficient toward NA) and other CYP enzymes in the lung may also be relevant.

Our data also show that the transgenic CYP2A13/2F1 can contribute to systemic disposition of circulating NA in humanized mice with compromised hepatic P450 function (Fig. 2E), but not in mice with normal hepatic P450 activity (Fig. 2G). It should be noted that the source of this extrahepatic contribution is most likely nasal mucosa, where the human transgene expression level (Wei et al., 2012) and NA metabolism activity (Table 1) were much higher than in lung. A dominant nasal (but not lung) contribution to NA disposition during postexposure period

would also explain the corresponding decreases in NA-GSH levels in the lung (Fig. 3F). In that connection, the persistence of in vivo NA-GSH formation in the lungs of "*Cyp2abfgs*-null and LCN" mice (Fig. 3D) demonstrated the ability of non-CYP2ABFGS enzymes of the lung to bioactivate NA in mice with deficient hepatic NA metabolism. Overall, the extrahepatic contributions to NA disposition were relatively small, insufficient to change circulating NA levels during active NA exposure (Fig. 2E, 0 h), or to cause significant changes in NA levels in the lung (Fig. 3E), contrary to the effects of LCN status (Fig. 2A, 2C, 3A, 3C).

The results of our recent study on the LCN mice (Kovalchuk et al., 2017) and of the present study on mouse models that are "humanized" by having a much lower overall rate of NA metabolism in the lung (relative to WT mice) and by expressing human CYP2A13 and CYP2F1 strongly support a protective role of hepatic P450 enzymes in reducing tissue burden and extent of bioactivation of NA in the lung, at least during the postexposure period. However, contrary to the expected protective role, LCN mice showed lower sensitivity to NA-induced lung toxicity than WT mice following inhalation exposure to NA at occupationally relevant concentrations; this fact suggested that liver P450-generated NA metabolites also contribute to toxicity in lung airways (Kovalchuk et al., 2017). Thus, it remains to be determined whether liver-produced reactive NA metabolites (e.g. NA-oxide and NA-quinones) can be transported to the lung, and whether deficiency of P450-mediated NA metabolism in the liver leads to decreases in the amount of these metabolites in the circulation and lung tissue. A more complete account of NA tissue burden and in situ bioactivation in the lung, as well as burden of systemically derived reactive NA metabolites, during and after NA inhalation exposure will facilitate establishment of accurate predictive models for risk assessment in humans.

In conclusion, we showed that a deficiency in hepatic NA metabolism not only decreases NA systemic disposition, but also causes NA to accumulate in tissues following inhalation exposure. Subsequent NA release from tissue is partly responsible for the prolonged occurrence of NA exposure and bioactivation in the lung after inhalation exposures have ceased. Our data also reveal ability of respiratory tract P450 enzyme to influence the rate of systemic NA disposition in mice with deficient hepatic P450 activity and support a dominant effect of the target tissue bioavailability of NA on extent of NA bioactivation in the lung. Furthermore, we demonstrate the ability of non-CYP2ABFGS enzymes of the lung to bioactivate NA in mice with deficient hepatic NA metabolism. Taken together, these results support the notion that assessment of toxic potential for naphthalene and other inhaled xenobiotics in human lungs should consider the balance between hepatic and lung P450's roles in both bioactivation and disposition, and they suggest potentially large effects of deficiencies in hepatic P450 activity on NA tissue burden and bioactivation in human lungs.

Acknowledgements

We thank Drs. Alan Buckpitt and Dexter Morin from University of California at Davis for providing NA-GSH standards. We also acknowledge Ms. Weizhu Yang for assistance with mouse breeding.

Authorship Contribution

Participated in research design: NK, QYZ, JK, LVW, XD

Conducted experiments: NK, JK

Performed data analysis: NK, JK, LVW, XD

Wrote or contributed to the writing of the manuscript: NK, QYZ, JK, LVW, XD

DMD Fast Forward. Published on October 8, 2019 as DOI: 10.1124/dmd.119.088930
This article has not been copyedited and formatted. The final version may differ from this version.

References

Abdo KM, Eustis S, McDonald M, Jokinen M, Adkins B, and Haseman J (1992) Naphthalene: A respiratory tract toxicant and carcinogen for mice. *Inhal Toxicol* **4:**393-409.

Abdo KM, Grumbein S, Chou BJ, and Herbert R (2001) Toxicity and carcinogenicity study in F344 rats following 2 years of whole-body exposure to naphthalene vapors. *Inhal Toxicol* **13:**931-950.

Buckpitt A, Boland B, Isbell M, Morin D, Shultz M, Baldwin R, Chan K, Karlsson A, Lin C, Taff A, West J, Fanucchi M, Van Winkle L, and Plopper C (2002) Naphthalene-induced respiratory tract toxicity: metabolic mechanisms of toxicity. *Drug Metab Rev* **34:**791-820.

Carr BA, Wan J, Hines RN, and Yost GS (2003) Characterization of the human lung CYP2F1 gene and identification of a novel lung-specific binding motif. *J Biol Chem* **278:**15473-15483.

Chao YC, Kupper LL, Serdar B, Egeghy PP, Rappaport SM, and Nylander-French LA (2006) Dermal exposure to jet fuel JP-8 significantly contributes to the production of urinary naphthols in fuel-cell maintenance workers. *Environ Health Perspect* **114:**182-185.

Cho TM, Rose RL, and Hodgson E (2006) In vitro metabolism of naphthalene by human liver microsomal cytochrome P450 enzymes. *Drug Metab Dispos* **34:**176-183.

Frye RF, Zgheib NK, Matzke GR, Chaves-Gnecco D, Rabinovitz M, Shaikh OS, and Branch RA (2006) Liver disease selectively modulates cytochrome P450--mediated metabolism. *Clin Pharmacol Ther* **80:**235-245.

Genter MB, Marlowe J, Kevin Kerzee J, Dragin N, Puga A, Dalton TP, and Nebert DW (2006) Naphthalene toxicity in mice and aryl hydrocarbon receptor-mediated CYPs. *Biochem Biophys Res Commun* **348:**120-123.

George J, Murray M, Byth K, and Farrell GC (1995) Differential alterations of cytochrome P450 proteins in livers from patients with severe chronic liver disease. *Hepatology* **21:**120-128.

Griego FY, Bogen KT, Price PS, and Weed DL (2008) Exposure, epidemiology and human cancer incidence of naphthalene. *Regul Toxicol Pharmacol* **51:**S22-26.

Gu J, Weng Y, Zhang QY, Cui H, Behr M, Wu L, Yang W, Zhang L, and Ding X (2003) Liver-specific deletion of the NADPH-cytochrome P450 reductase gene: impact on plasma cholesterol homeostasis and the function and regulation of microsomal cytochrome P450 and heme oxygenase. *J Biol Chem* **278:**25895-25901.

Hu J, Sheng L, Li L, Zhou X, Xie F, D'Agostino J, Li Y, and Ding X (2014) Essential role of the cytochrome P450 enzyme CYP2A5 in olfactory mucosal toxicity of naphthalene. *Drug Metab Dispos* **42:**23-27.

Kakareka SV and Kukharchyk TI (2003) PAH emission from the open burning of agricultural debris. *Sci Total Environ* **308:**257-261.

Kovalchuk N, Kelty J, Li L, Hartog M, Zhang QY, Edwards P, Van Winkle L, and Ding X (2017) Impact of hepatic P450-mediated biotransformation on the disposition and respiratory tract toxicity of inhaled naphthalene. *Toxicol Appl Pharmacol* **329:**1-8.

Li L, Carratt S, Hartog M, Kovalchik N, Jia K, Wang Y, Zhang QY, Edwards P, Winkle LV, and Ding X (2017) Human CYP2A13 and CYP2F1 Mediate Naphthalene Toxicity in the Lung and Nasal Mucosa of CYP2A13/2F1-Humanized Mice. *Environ Health Perspect* **125:**067004.

Li L, Megaraj V, Wei Y, and Ding X (2014) Identification of cytochrome P450 enzymes critical for lung tumorigenesis by the tobacco-specific carcinogen 4-(methylnitrosamino)-1-(3-pyridyl)-1-butanone (NNK): insights from a novel Cyp2abfgs-null mouse. *Carcinogenesis* **35:**2584-2591.

Li L, Wei Y, Van Winkle L, Zhang QY, Zhou X, Hu J, Xie F, Kluetzman K, and Ding X (2011) Generation and characterization of a Cyp2f2-null mouse and studies on the role of CYP2F2 in naphthalene-induced toxicity in the lung and nasal olfactory mucosa. *J Pharmacol Exp Ther* **339:**62-71.

McClean MD, Osborn LV, Snawder JE, Olsen LD, Kriech AJ, Sjodin A, Li Z, Smith JP, Sammons DL, Herrick RF, and Cavallari JM (2012) Using urinary biomarkers of polycyclic aromatic compound exposure to guide exposure-reduction strategies among asphalt paving workers. *Ann Occup Hyg* **56:**1013-1024.

Merchant-Borna K, Rodrigues EG, Smith KW, Proctor SP, and McClean MD (2012) Characterization of inhalation exposure to jet fuel among U.S. Air Force personnel. *Ann Occup Hyg* **56:**736-745.

Preuss R, Angerer J, and Drexler H (2003) Naphthalene--an environmental and occupational toxicant. *Int Arch Occup Environ Health* **76:**556-576.

Richieri PR and Buckpitt AR (1987) Efflux of naphthalene oxide and reactive naphthalene metabolites from isolated hepatocytes. *J Pharmacol Exp Ther* **242:**485-492.

Serdar B, Egeghy PP, Gibson R, and Rappaport SM (2004) Dose-dependent production of urinary naphthols among workers exposed to jet fuel (JP-8). *Am J Ind Med* **46:**234-244.

Shimada T, Takenaka S, Kakimoto K, Murayama N, Lim YR, Kim D, Foroozesh MK, Yamazaki H, Guengerich FP, and Komori M (2016) Structure-Function Studies of Naphthalene, Phenanthrene, Biphenyl, and Their Derivatives in Interaction with and Oxidation by Cytochromes P450 2A13 and 2A6. *Chem Res Toxicol* **29:**1029-1040.

Shultz MA, Choudary PV, and Buckpitt AR (1999) Role of murine cytochrome P-450 2F2 in metabolic activation of naphthalene and metabolism of other xenobiotics. *J Pharmacol Exp Ther* **290:**281-288.

Su T, Bao Z, Zhang QY, Smith TJ, Hong JY, and Ding X (2000) Human cytochrome P450 CYP2A13: predominant expression in the respiratory tract and its high efficiency metabolic activation of a tobacco-specific carcinogen, 4-(methylnitrosamino)-1-(3-pyridyl)-1-butanone. *Cancer Res* **60:**5074-5079.

Tingle MD, Pirmohamed M, Templeton E, Wilson AS, Madden S, Kitteringham NR, and Park BK (1993) An investigation of the formation of cytotoxic, genotoxic, protein-reactive and stable metabolites from naphthalene by human liver microsomes. *Biochem Pharmacol* **46:**1529-1538.

Verschoyle RD, Martin J, and Dinsdale D (1997) Selective inhibition and induction of CYP activity discriminates between the isoforms responsible for the activation of butylated hydroxytoluene and naphthalene in mouse lung. *Xenobiotica* **27:**853-864.

Warren DL, Brown DL, Jr., and Buckpitt AR (1982) Evidence for cytochrome P-450 mediated metabolism in the bronchiolar damage by naphthalene. *Chem Biol Interact* **40:**287-303.

Weems JM and Yost GS (2010) 3-Methylindole metabolites induce lung CYP1A1 and CYP2F1 enzymes by AhR and non-AhR mechanisms, respectively. *Chem Res Toxicol* **23:**696-704.

Wei Y, Wu H, Li L, Liu Z, Zhou X, Zhang QY, Weng Y, D'Agostino J, Ling G, Zhang X, Kluetzman K, Yao Y, and Ding X (2012) Generation and characterization of a CYP2A13/2B6/2F1-transgenic mouse model. *Drug Metab Dispos* **40:**1144-1150.

Wilson AS, Davis CD, Williams DP, Buckpitt AR, Pirmohamed M, and Park BK (1996) Characterisation of the toxic metabolite(s) of naphthalene. *Toxicology* **114:**233-242.

Witschi H, Espiritu I, Maronpot RR, Pinkerton KE, and Jones AD (1997) The carcinogenic potential of the gas phase of environmental tobacco smoke. *Carcinogenesis* **18:**2035-2042.

Wu L, Gu J, Weng Y, Kluetzman K, Swiatek P, Behr M, Zhang QY, Zhuo X, Xie Q, and Ding X (2003) Conditional knockout of the mouse NADPH-cytochrome p450 reductase gene. *Genesis* **36:**177-181.

Footnotes

This work was supported in part by the National Institutes of Health [Grants ES020867, ES023513, ES006694, HL007013 (NHLBI T32 to Jacklyn Kelty)].

DMD Fast Forward. Published on October 8, 2019 as DOI: 10.1124/dmd.119.088930
This article has not been copyedited and formatted. The final version may differ from this version.

Legend to Figures

Fig. 1. Production and analysis of mouse models used in this study. **A.** Breeding scheme for generation of CYP2A13/2F1-humanized mice with either normal or abolished hepatic CPR expression. The original *Cyp2abfgs*$^{-/-}$, Alb-Cre$^{+/-}$/*Cpr*$^{lox/lox}$ (LCN), and CYP2A13/2F1$^{+/-}$/*Cyp2abfgs*$^{-/-}$ (CYP2A13/2F1-humanized) strains were intercrossed to yield the four desired genotypes for this study. All mice are on the C57BL/6 genetic background. **B**. Representative results of PCR-based genotyping to identify presence of various alleles, including *Cyp2abfgs*$^{-}$, Alb-Cre^{+}, *Cpr*^{lox}, *Cpr*$^{+}$, *Cyp2f2*$^{+}$ (representing the *Cyp2abfgs* gene cluster), and *CYP2F1*$^{+}$ (representing both CYP2A13 and 2F1). The PCR primers used for the genotyping methods are listed in Supplementary Table 1. Positive controls (Pos) were derived from genomic DNA from *Alb-Cre*$^{+/-}$*Cpr*$^{lox/+}$ mice, for Alb-*Cre*$^{+}$, *Cpr*$^{+}$, *Cpr*^{lox}, and *Cyp2f2*, or from CYP2A13/2F1-TG$^{+/-}$/*Cyp2abfgs*$^{-/-}$ mice, for *Cyp2abfgs*$^{-}$ and *CYP2F1*$^{+}$. Negative controls (Neg) were derived from reactions without an added DNA template. PCR products were analyzed and visualized as described in Materials and Methods.

Fig. 2. Levels of NA and NA-GSH in the plasma. Two-month old CYP2A13/2F1-humanized, "CYP2A13/2F1-humanized and LCN" (A, B), or *Cyp2abfgs*-null and "*Cyp2abfgs-null* and LCN" (C, D), male mice (n=3-4 per genotype) were simultaneously exposed to 10 ppm of NA for 4 hours as described in Materials and Methods. Plasma levels of NA (A, C, E, G) and NA-GSH (B, D, F, H) were determined at different time points after termination of NA exposure. Data from A-D are replotted in E-H. Data represent means ± S.D. (n=3-4). *, ***, ****, $p<0.05$, 0.001, or 0.0001, respectively, compared by genotype (two-way ANOVA followed by Bonferroni's test for multiple comparisons).

Fig. 3. Levels of NA and NA-GSH in the lung. Two-month old CYP2A13/2F1-humanized, "CYP2A13/2F1-humanized and LCN" (A, B), or *Cyp2abfgs*-null and "*Cyp2abfgs*-null and LCN" (C, D) male mice (n=3-5 per genotype for each time point) were exposed to 10 ppm of NA for 4 hours. Lungs were collected 0, 2, 6, or 20 hours after termination of NA exposure. Levels of NA (A, C, E, G) and NA-GSH (B, D, F, H) in tissue homogenates were determined. Data from A-D are replotted in E-H. Data represent means ± S.D. (n=3-5). ***, $p<0.001$; **, $p<0.01$; compared between genotypes for the corresponding time point; ^^^^, $p<0.0001$; ^^, $p<0.01$; ^$p<0.05$; compared to 0 hour, for the corresponding genotype (two-way ANOVA followed by Bonferroni's test for multiple comparisons). N.D., below detection limit.

Fig. 4. Comparison of NA and NA-GSH levels in lung and plasma at 0-h postexposure. Data from Figures 2 and 3 are re-plotted for a direct comparison between lung and plasma. Data represent means ± S.D. (n=3-5). *, $p<0.05$; **, $p<0.01$; compared between lung and plasma for the corresponding genotype (two-way ANOVA followed by Bonferroni's test for multiple comparisons).

Fig. 5. Levels of NA and NA-GSH in the liver. Two-month old CYP2A13/2F1-humanized, "CYP2A13/2F1-humanized and LCN" (A), *Cyp2abfgs*-null and "*Cyp2abfgs*-null and LCN" (B) male mice (n=3-5 per genotype for each time point) were exposed to 10 ppm of NA for 4 h. Livers from the same groups of mice described in Figure 3 were collected for determination of NA (A, C, E, G) and NA-GSH (B, D, F, H) in tissue homogenates. Data from A-D are replotted in E-H. Data represent means ± S.D. (n=3-5). ****, $p<0.0001$; compared between genotypes for the

corresponding time point; ^^^^, p<0.0001; ^^, p<0.01; ^p<0.05; compared to 0 hour, for the corresponding genotype (two-way ANOVA followed by Bonferroni's test for multiple comparisons).

Fig. 6. Comparison of NA and NA-GSH levels in liver and lung at 0-h postexposure. Data from Figures 3 and 5 are re-plotted for a direct comparison between liver and lung. Data represent means ± S.D. (n=3-5). *, p<0.05; ****, p<0.0001; compared between liver and lung for the corresponding genotype; ^^^^, p<0.0001; compared between CYP2A13/2F1-humanized and *Cyp2abfgs*-null mice with either normal or abolished hepatic CPR activity (two-way ANOVA followed by Bonferroni's test for multiple comparisons).

DMD Fast Forward. Published on October 8, 2019 as DOI: 10.1124/dmd.119.088930
This article has not been copyedited and formatted. The final version may differ from this version.

TABLE 1

Metabolic activity of nasal mucosa, lung and liver microsomes of "CYP2A13/2F1-humanized and LCN" and "*Cyp2abfgs*-null and LCN" mice *in vitro*

Rates of formation of NA-GSH was determined as described in Material and Methods. Reaction mixtures contained 50 mM phosphate buffer (pH 7.4), 10 mM GSH, 1 mM NADPH, various concentrations of microsomal proteins (0.2 mg/mL for individual livers, 0.25 mg/mL for pooled olfactory mucosa, and 1 mg/mL for pooled lung), and NA at 100 μM. The values represent means ± S.D. (n=3-4). Statistical analysis was performed using two-way ANOVA followed by Bonferroni's test for multiple comparisons. Previously reported data for LCN, *Cyp2abfgs*-null, and CYP2A13/2F1-humanized mice (Kovalchuk et al., 2017; Li et al., 2017) are shown for comparison.

Tissue	Rates of NA-GSH formation (pmol/min/mg of microsomal protein)				
	"CYP2A13/2F1-humanized and LCN"	"*Cyp2abfgs*-null and LCN"	CYP2A13/2F1-humanized[a]	*Cyp2abfgs*-null[a]	LCN[b]
Nasal mucosa	801 ± 77	206 ± 6[c]	964 ± 59	118 ± 12	N.A.[d]
Lung	19.9 ± 4.9	11.9 ± 0.5[e]	23.1 ± 3.2	8.1 ± 0.5	1120 ± 198
Liver	76.9 ± 13.5	94.7 ± 26.3	N.A.	N.A.	83.7 ± 8.7

[a]Extracted from Figure 1 of (Li et al., 2017), for rates at 100 μM NA

[b]From original data used for kinetic analysis in Table 1 of (Kovalchuk et al., 2017), for rates at 100 μM NA

[c]$p<0.0001$, compared to "CYP2A13/2F1-humanized and LCN"

[d]N.A., not analyzed

[e]$p<0.05$, compared to "CYP2A13/2F1-humanized and LCN"

DMD Fast Forward. Published on October 8, 2019 as DOI: 10.1124/dmd.119.088930
This article has not been copyedited and formatted. The final version may differ from this version.

TABLE 2

Toxicokinetic parameters of plasma NA and NA-GSH in *Cyp2abfgs*-null, CYP2A13/2F1-humanized, "*Cyp2abfgs*-null and LCN" and "CYP2A13/2F1-humanized and LCN" mice

Data from Figure 2 are used for calculation of various toxicokinetic parameters. Results are presented as means ± S.D. (n=3-4 per group).

Analyte	Strain	$AUC_{0\text{-}20h}$, µg•min/ml	$t_{1/2}$, min	CL/F, ml/min	C_{max}, ng/ml
NA	*Cyp2abfgs*-null	4.2 ± 0.9	3.5 ± 1.4	72.3 ± 17.7	80.3 ± 26.5
	CYP2A13/2F1-humanized	4.6 ± 3.9	3.2 ± 1.1	122 ± 78	67.6 ± 20.2
	"*Cyp2abfgs*-null and LCN"	280 ± 40[a]	43 ± 11	1.1 ± 0.3[b]	226 ± 43[a]
	"CYP2A13/2F1-humanized and LCN"	170 ± 20[c, d]	57 ± 39	1.9 ± 0.2[c]	192 ± 49[c]
NA-GSH	*Cyp2abfgs*-null	5.2 ± 1.1	N/A	N/A	48.0 ± 20.1
	CYP2A13/2F1-humanized	3.2 ± 2.6	N/A	N/A	51.6 ± 18.4
	"*Cyp2abfgs*-null and LCN"	30 ± 4[b]	N/A	N/A	38.8 ±5.7
	"CYP2A13/2F1-humanized and LCN"	26 ± 8[e]	N/A	N/A	25.7 ± 14.3

[a]p<0.0001, compared to *Cyp2abfgs*-null

[b]p< 0.05, compared to *Cyp2abfgs*-null

[c]p<0.0001, compared to CYP2A13/2F1-humanized

[d]p<0.001, compared to "*Cyp2abfgs*-null and LCN"

[e]p<0.05, compared to CYP2A13/2F1-humanized

N/A, not applicable

DMD Fast Forward. Published on October 8, 2019 as DOI: 10.1124/dmd.119.088930
This article has not been copyedited and formatted. The final version may differ from this version.

Figure 1

A

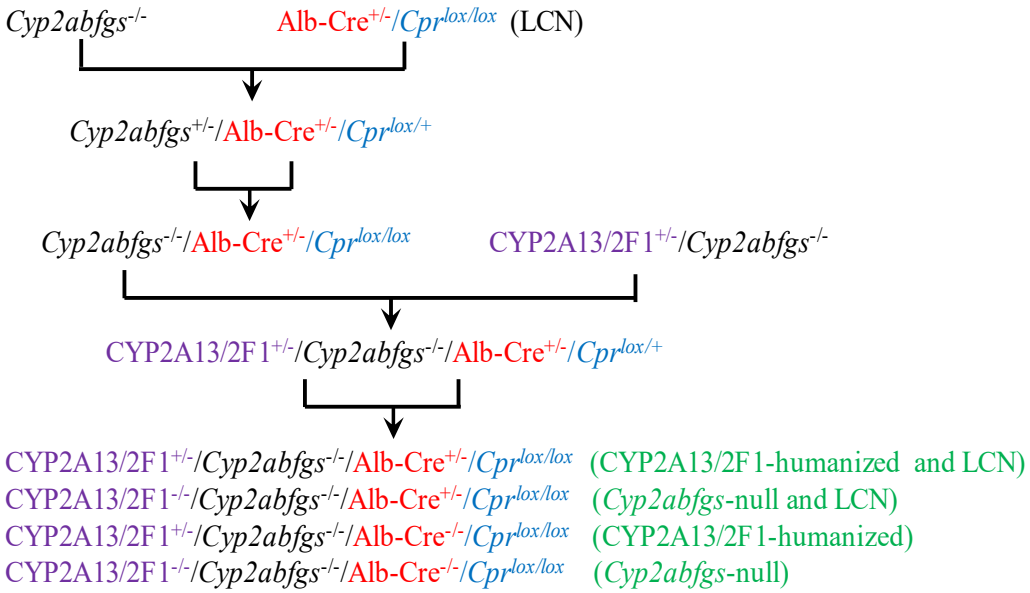

B

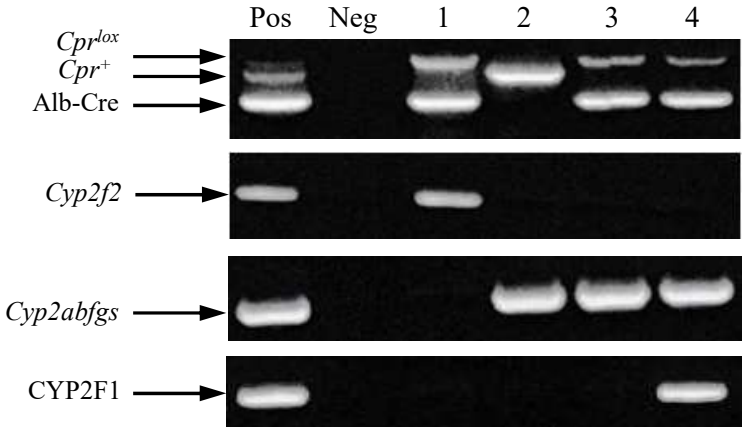

1 – Alb-Cre+/-/Cprlox/lox (LCN)
2 – *Cyp2abfgs*-null
3 – *Cyp2abfgs*-null and LCN
4 – CYP2A13/2F1-humanized and LCN

DMD Fast Forward. Published on October 8, 2019 as DOI: 10.1124/dmd.119.088930
This article has not been copyedited and formatted. The final version may differ from this version.

Figure 2

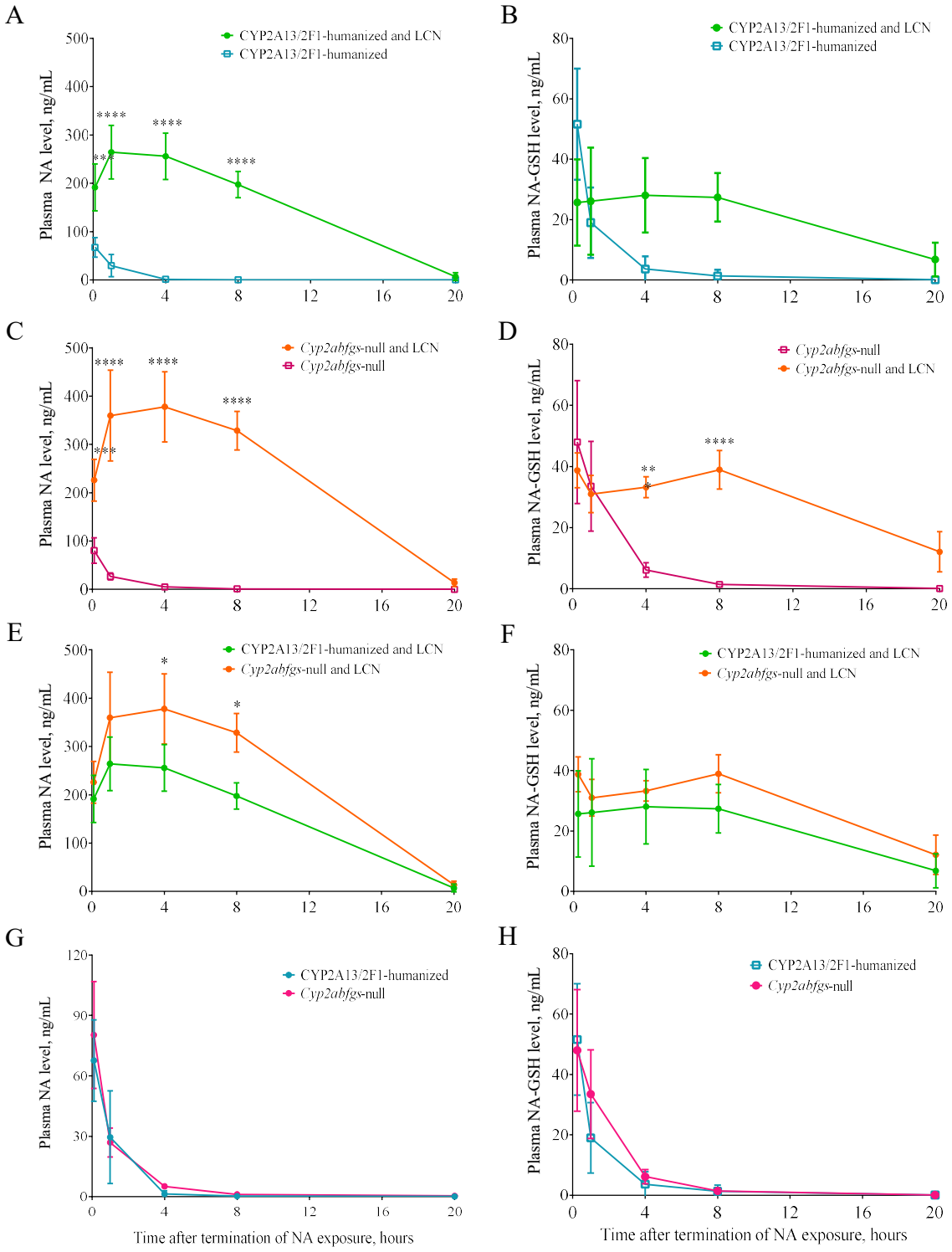

DMD Fast Forward. Published on October 8, 2019 as DOI: 10.1124/dmd.119.088930
This article has not been copyedited and formatted. The final version may differ from this version.

Figure 3

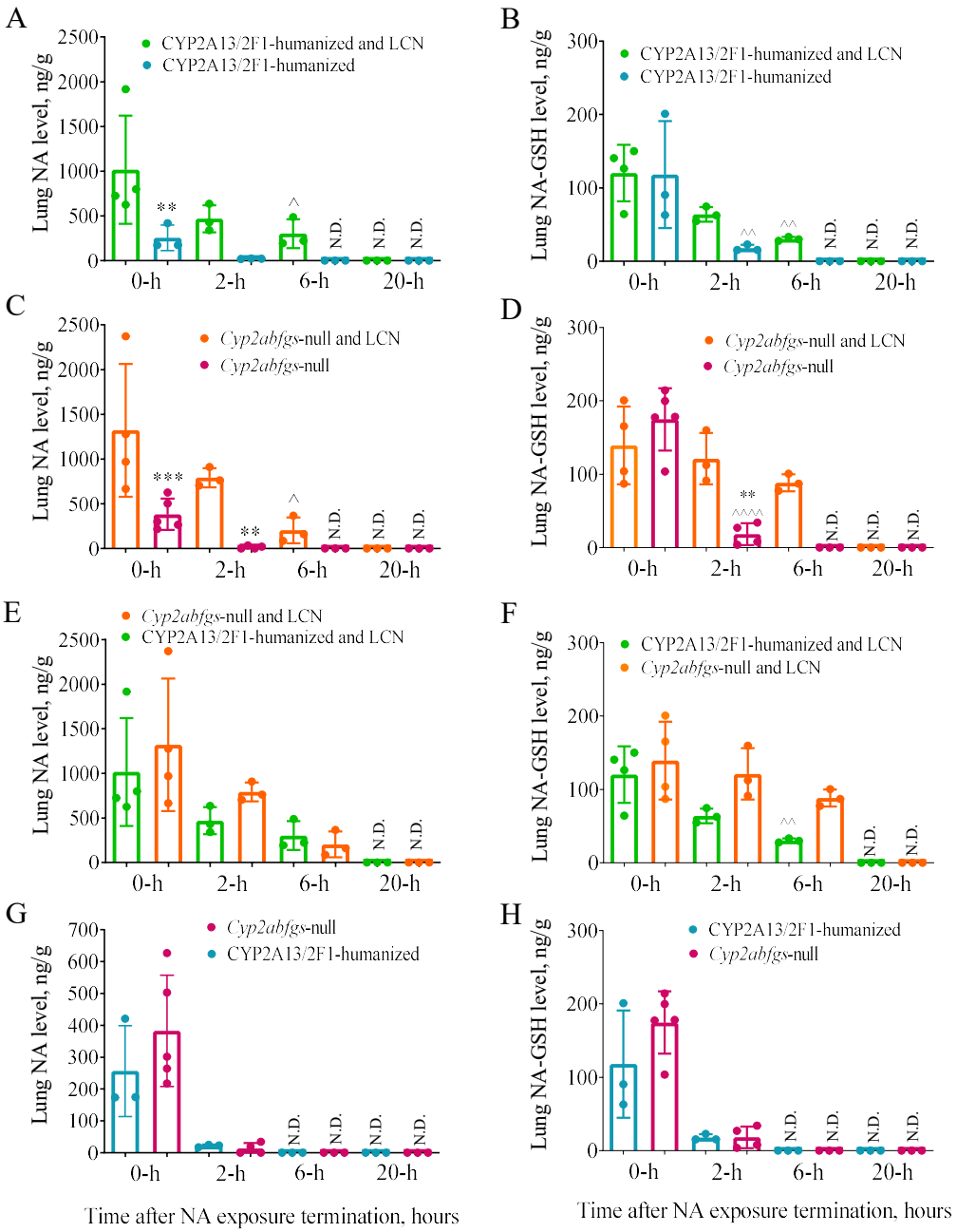

DMD Fast Forward. Published on October 8, 2019 as DOI: 10.1124/dmd.119.088930
This article has not been copyedited and formatted. The final version may differ from this version.

Figure 4

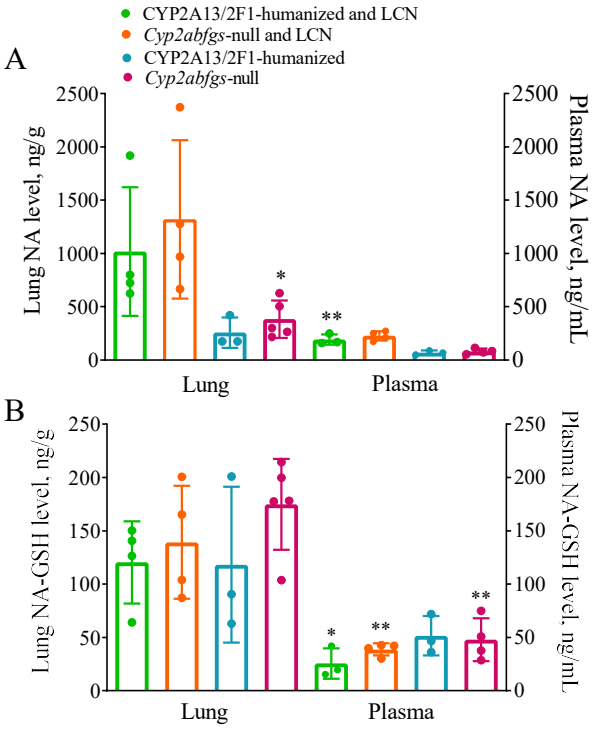

DMD Fast Forward. Published on October 8, 2019 as DOI: 10.1124/dmd.119.088930
This article has not been copyedited and formatted. The final version may differ from this version.

Figure 5

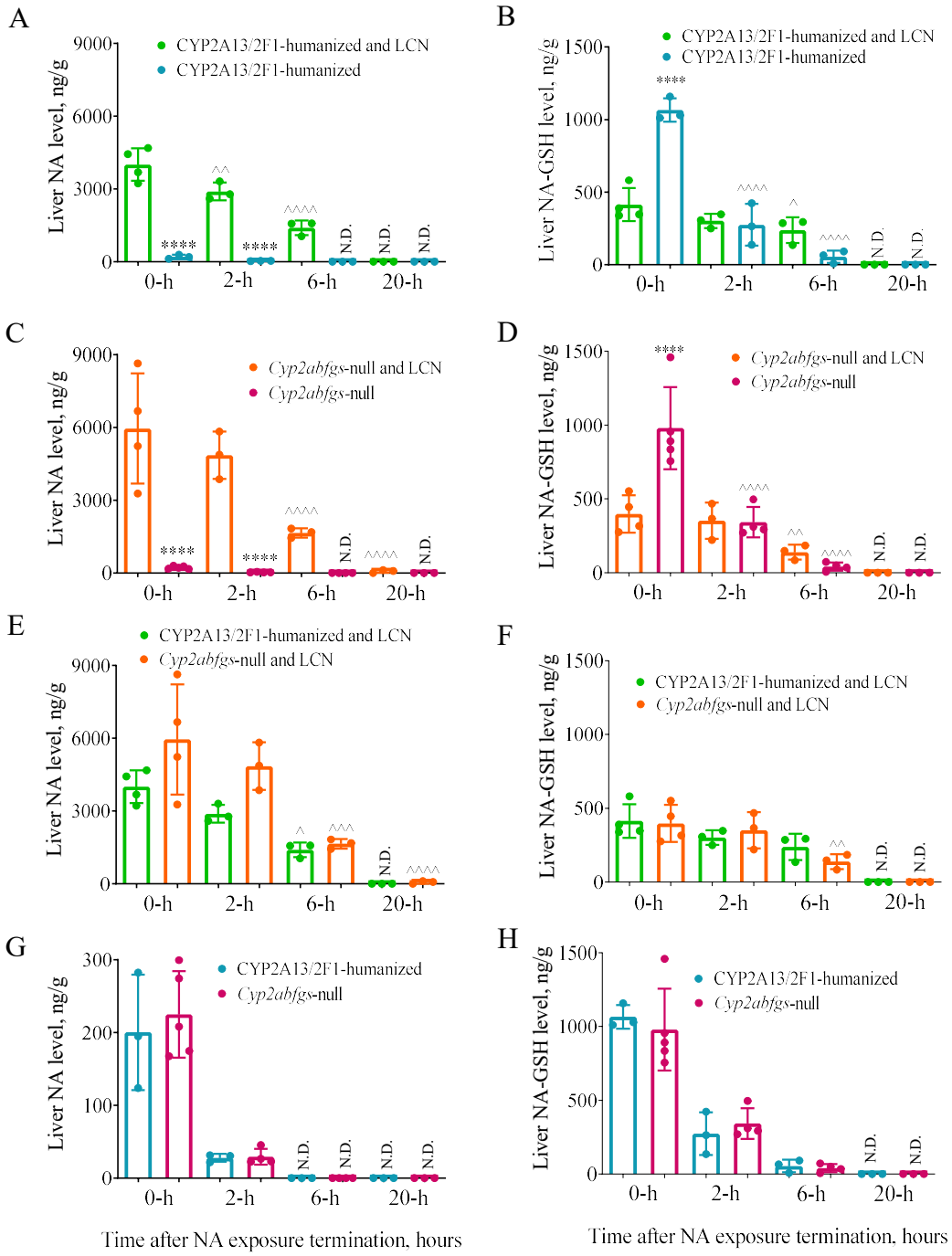

DMD Fast Forward. Published on October 8, 2019 as DOI: 10.1124/dmd.119.088930
This article has not been copyedited and formatted. The final version may differ from this version.

Figure 6

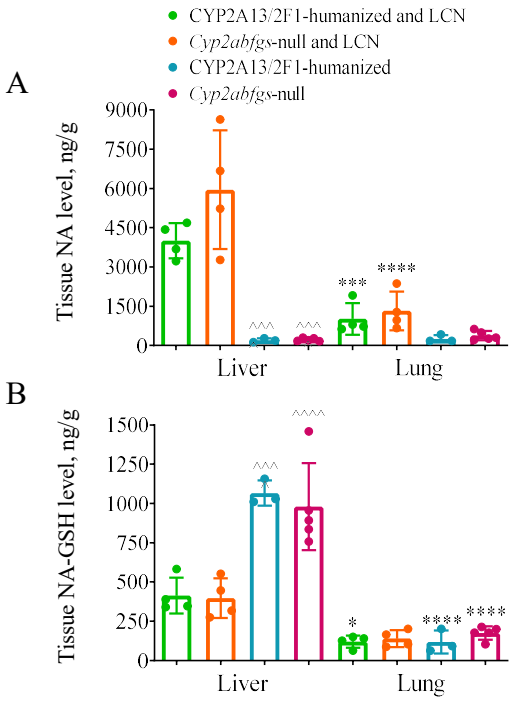

(Drug Metabolism and Disposition)

Supplemental Material

Toxicokinetic interaction between hepatic disposition and pulmonary bioactivation of inhaled naphthalene studied using *Cyp2abfgs*-null and CYP2A13/2F1-humanized mice with deficient hepatic cytochrome P450 activity

Nataliia Kovalchuk, Qing-Yu Zhang, Jacklyn Kelty, Laura Van Winkle, and Xinxin Ding

Department of Pharmacology and Toxicology, College of Pharmacy, University of Arizona, Tucson, AZ 85721 (N.K., Q.-Y.Z., X.D.); Wadsworth Center, New York State Department of Health, and School of Public Health, State University of New York at Albany, NY 12201 (N.K., Q.-Y.Z.); Center for Health and the Environment and Department of Anatomy Physiology and Cell Biology, School of Veterinary Medicine UC Davis, Davis, CA 95616 (J.K., L.V.); College of Nanoscale Science, SUNY Polytechnic Institute, Albany, NY 12203 (X.D.)

Supplementary TABLE 1

Primers used for PCR-based genotype analysis

Allele	Sequence of forward primer	Sequence of reverse primer	Reference
Cre^{+}	5'-gga ttt ccg tct ctg gtg tag c-3'	5'-cat tgc ccc tgt ttc act atc c-3'	(Wei et al., 2013)
Cpr-Lox	5'-aag agg gac aaa gag cac c-3'	5'-tac aat gga cca ggc tct gc-3'	(Wu et al., 2003)
Cyp2f2^{+}	5'-aga gat gac tcg gtg gct gt-3'	5'-ttt ttc cca tgc caa agt tc-3'	(Li et al., 2011)
Cyp2abfgs^{-}	5'-caa gcc atg ttt ttg ttg ga-3'	5'-ctc cct ggg atg gga act at-3'	(Li et al., 2014)
$CYP2F1^{+}$	5'-aac ctc atc tta tct cac cg-3'	5'-cat cgc tca cag gcg aat c-3'	(Jia et al., 2014)

Supplementary TABLE 2

Body and organ weights

Naïve 2-3-month-old *Cyp2abfgs*-null, CYP2A13/2F1-humanized, "*Cyp2abfgs*-null-and-LCN", and "CYP2A13/2F1-humanized-and-LCN" male mice on C57BL/6 genetic background were compared. All data are expressed as means ± S.D. (n=3).

Mouse genotype	Body, g	Lung, g	Liver, g	Kidney, g	Brain, g	Heart, g
Cyp2abfgs-null	23.3±1.8	0.16±0.02	1.25±0.12	0.32±0.02	0.39±0.06	0.13±0.01
CYP2A13/2F1-humanized	23.7±2.8	0.15±0.02	1.21±0.11	0.34±0.03	0.41±0.03	0.14±0.02
"*Cyp2abfgs*-null-and-LCN"	24.4±3.3	0.15±0.02	1.98±0.33[a]	0.34±0.04	0.42±0.02	0.13±0.02
"CYP2A13/2F1-humanized-and-LCN"	23.2±0.7	0.16±0.01	2.12±0.18[a]	0.33±0.01	0.40±0.03	0.13±0.02

[a]$p<0.05$; for comparisons between *Cyp2abfgs*-null and "*Cyp2abfgs*-null-and-LCN", or between CYP2A13/2F1-humanized and "CYP2A13/2F1-humanized-and-LCN", mice. Student's *t* test.

Legends for Supplementary Figures

Supplementary Figure 1. Expression of hepatic CPR protein in various mouse strains. Hepatic microsomes (10 μg each) from naïve, male mice were used for immunoblot analysis for CPR and calnexin (as a loading control). Microsomes were prepared and subjected to immunoblot analysis as described previously (Ding and Coon, 1990). Two identical sets of four samples were analyzed on the same gel and transferred to nitrocellulose membrane, which was then cut vertically along the blue line into two parts for separate incubation (overnight at 4 ºC) with rabbit anti-rat cytochrome P450 reductase (Enzo Life Science, Plymouth, PA; lot # 06011013) or rabbit anti-human calnexin (GenScript, Piscataway, NJ), as a marker protein for the endoplasmic reticulum, as indicated. Peroxidase-conjugated goat anti-rabbit IgG (Sigma-Aldrich, lot #A4914) was used as the secondary antibody. The immunoreactive signal was detected with a chemiluminescence kit (GE Healthcare, Piscataway, NJ). The two parts of the blot were realigned at the blue line before visualization using the Molecular Imager® Gel Doc™ XR+ System (Bio-Rad, Hercules, CA). Typical results are shown. The results confirm the expected loss of hepatocyte CPR protein expression in mice having the Alb-Cre$^{+/-}$/*Cpr*$^{lox/lox}$ genotype.

Supplementary Figure 2. Serum biochemical indicators in mice of different genotypes. Serum (100 μl each) from naïve *Cyp2abfgs*-null, CYP2A13/2F1-humanized, "*Cyp2abfgs*-null and LCN" and "CYP2A13/2F1-humanized and LCN" male mice were analyzed as described in Materials and Methods. All data are expressed as means ± S.D. (n=3). *, $p<0.05$; **, $p<0.01$; ****, $p<0.0001$, for comparisons between *Cyp2abfgs*-null and "*Cyp2abfgs*-null-and-LCN", or between CYP2A13/2F1-humanized and "CYP2A13/2F1-humanized-and-LCN", mice. Student's *t* test.

Supplementary Figure 1

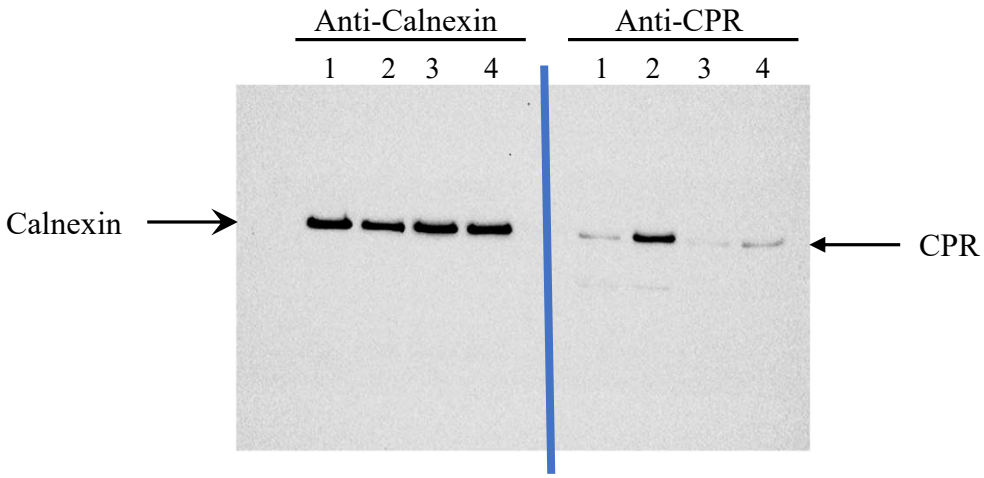

1 – Alb-Cre$^{+/-}$/*Cpr*$^{lox/lox}$ (LCN)
2 – *Cyp2abfgs*-null
3 – *Cyp2abfgs*-null and LCN
4 – CYP2A13/2F1-humanized and LCN

Supplementary Figure 2

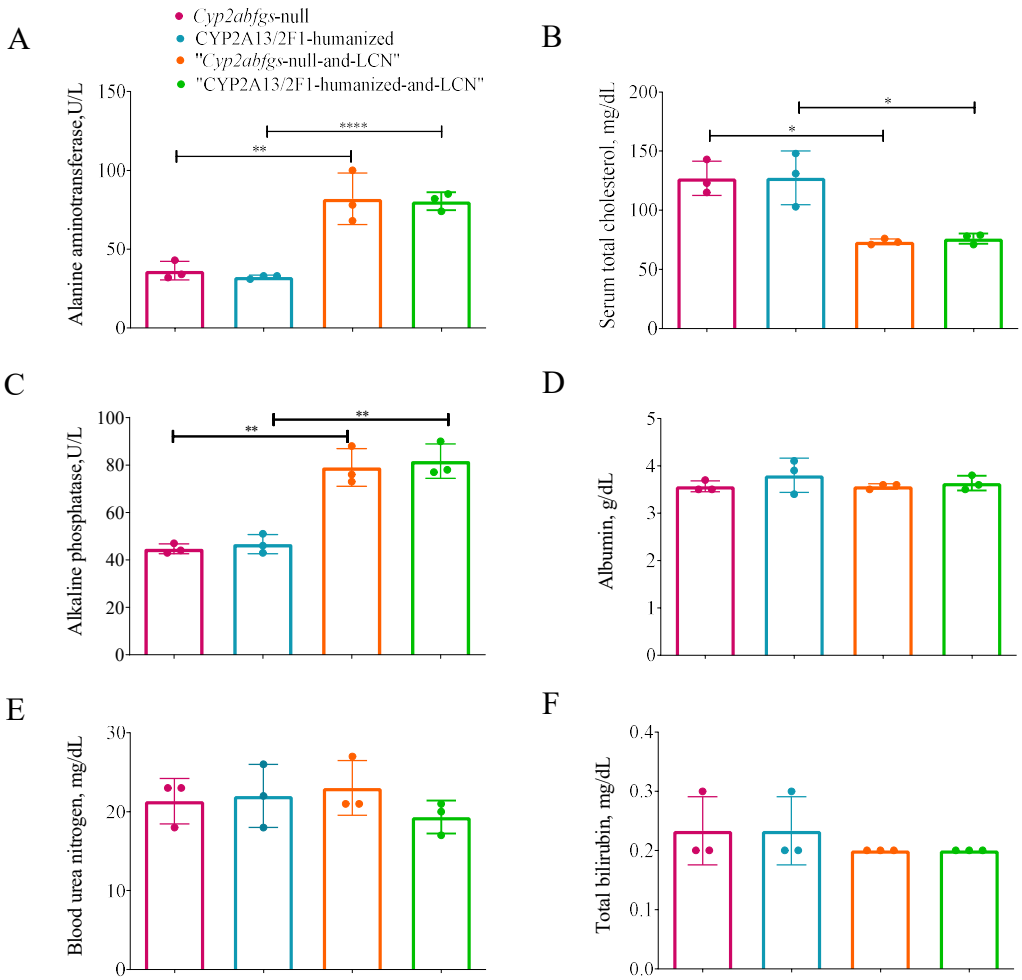

References

Ding X and Coon MJ (1990) Immunochemical characterization of multiple forms of cytochrome P-450 in rabbit nasal microsomes and evidence for tissue-specific expression of P-450s NMa and NMb. *Mol Pharmacol* **37:**489-496.

Jia K, Li L, Liu Z, Hartog M, Kluetzman K, Zhang QY, and Ding X (2014) Generation and characterization of a novel CYP2A13--transgenic mouse model. *Drug Metab Dispos* **42:**1341-1348.

Li L, Megaraj V, Wei Y, and Ding X (2014) Identification of cytochrome P450 enzymes critical for lung tumorigenesis by the tobacco-specific carcinogen 4-(methylnitrosamino)-1-(3-pyridyl)-1-butanone (NNK): insights from a novel Cyp2abfgs-null mouse. *Carcinogenesis* **35:**2584-2591.

Li L, Wei Y, Van Winkle L, Zhang QY, Zhou X, Hu J, Xie F, Kluetzman K, and Ding X (2011) Generation and characterization of a Cyp2f2-null mouse and studies on the role of CYP2F2 in naphthalene-induced toxicity in the lung and nasal olfactory mucosa. *J Pharmacol Exp Ther* **339:**62-71.

Wei Y, Li L, Zhou X, Zhang QY, Dunbar A, Liu F, Kluetzman K, Yang W, and Ding X (2013) Generation and characterization of a novel Cyp2a(4/5)bgs-null mouse model. *Drug Metab Dispos* **41:**132-140.

Wu L, Gu J, Weng Y, Kluetzman K, Swiatek P, Behr M, Zhang QY, Zhuo X, Xie Q, and Ding X (2003) Conditional knockout of the mouse NADPH-cytochrome p450 reductase gene. *Genesis* **36:**177-181.